Title

Fluorinated End-Groups in Electrolytes Induce Ordered Electrolyte/Anode Interface Even at Open-Circuit Potential as Revealed by Sum Frequency Generation Vibrational Spectroscopy

Journal

Advanced Energy Materials, 7(17)

ISSN

1614-6832

Authors

Horowitz, Yonatan
Han, Hui-Ling
Ralston, Walter T
et al.

Publication Date

2017-09-01

DOI

10.1002/aenm.201602060

Peer reviewed

Fluorinated End Groups in Electrolytes Induce Ordered Electrolyte / Anode Interface Even at Open Circuit Potential as Revealed by Sum Frequency Generation Vibrational Spectroscopy

Yonatan Horowitz[†,‡,*], Hui-Ling Han[‡,*], Walter T. Ralston[†,‡], Joyce Rodrigues de Araujo[‡,¶], Eric Kreidler[§], Chris Brooks[§] and Gabor A. Somorjai[†,‡,$]

[†]Department of Chemistry, University of California, Berkeley, California 94720, United States

[‡]Materials Sciences Division, Lawrence Berkeley National Laboratory, 1 Cyclotron Road, Berkeley, California 94720, United States

[¶]Materials Metrology Division, National Institute of Metrology, Quality and Technology, Duque de Caxias, Rio de Janeiro 25250-020, Brazil

[§]Honda Research Institute, Inc., 1381 Kinnear Road, Columbus, Ohio 43212, United States

ABSTRACT: Fluorine based additives have a tremendously beneficial effect on the performance of lithium ion batteries, yet the origin of this phenomenon is unclear. In this paper we show that the formation of a solid electrolyte interphase (SEI) on the anode surface in the first 5 charge / discharge cycles is affected by the stereochemistry of the electrolyte molecules on the anode surface starting at open circuit potential. We have studied an anode specific model system, the reduction of 1,2-diethoxy ethane with LiTFSI, lithium Bis(trifluoromethane)sulfonimide, as salt on amorphous silicon anode and compared the electrochemical response and SEI formation to its fluorinated version BTFEOE, Bis(2,2,2-trifluoroethoxy) ethane by sum frequency generation (SFG) vibrational spectroscopy under reaction conditions. Our SFG results suggest that the -CF_3 end groups of the linear ether BTFEOE change its adsorption orientation on the a-Si surface at open circuit potential, leading to a better protective layer. Supporting evidence from ex situ scanning electron microscopy (SEM) and X-ray photoelectron spectroscopy (XPS) depth profiling measurements show that the fluorinated ether, BTFEOE, yields a smooth SEI on the a-Si surface and enables lithium ion to intercalate deeper into the a-Si bulk.

1. INTRODUCTION

Upon charging a lithium-ion battery the electrolyte solution is reduced on the anode and forms a solid electrolyte interphase (SEI).[1] The reduction products of the electrolyte forming the SEI are dependent on the electrolyte composition and anode material.[2],[3] Notably, the addition of fluorinated electrolyte to the electrolyte solution results in improved cyclability[4] and lower irreversible capacity loss.[5] Ethers, once candidates for commercial electrolytes, have lost their appeal due to their instability at lower oxidation potentials compared with alkyl-carbonates[6], yet have regained interest[7] as solvents in lithium-oxygen[8], solid lithium anode[9] and beyond lithium batteries.[10] Nevertheless, to better understand the different solid electrolyte interphase formation mechanism of hydrocarbon vs. fluorinated electrolytes on anodes we propose a simplified electrochemical system of a single solvent electrolyte 1,2-DEE and its fluorinated compound BTFEOE, Bis(2,2,2-trifluoroethoxy) ethane in contact with amorphous silicon. We chose LiTFSI as salt due to its counter anions' high solubility and relative high stability in linear ethers[11] and to reduce LiF formation.[12] In order to investigate the effect of electrolyte on the properties of a silicon anode surface, we use sum frequency generation (SFG) vibrational spectroscopy, which is a non-linear optical technique that yields vibrational spectra of molecules at interfaces.[13] Previously, SFG has been applied in order to investigate electrolyte orientation and surface concentration[14],[15] and electrochemical processes in battery systems.[16],[17],[18]

In order to study the SEI formation mechanism on Si anode surfaces with SFG, we chose to use 200 nm thick amorphous silicon (a-Si) films. The

choice of an amorphous Si thin film provides several important advantages: (1) it is highly transparent to the incoming infra-red and visible beams, as well as, to the reflected SFG beam allow us to probe the interface without suffering the electrolyte absorption;[20] (2) we avoided mechanical failure due to volume expansion (upon lithiation)[19],[20]; and (3) minimize phase transition from amorphous to crystalline phase ($Li_{15}Si_4$) upon lithiation.[21],[22]

In this fundamental work, we present the effect of fluorinated electrolytes even at open circuit potential (i.e., no applied potential) in a simplified battery system on the formation of the SEI as well as on lithium diffusion into the silicon bulk. We first probe the amorphous silicon / electrolyte interphase at open circuit potentials, followed by probing SEI formation under working conditions by SFG vibrational spectroscopy. Then, we further examine the amorphous silicon surface morphology by scanning electron microscopy (SEM) and its chemistry by X-ray photoelectron spectroscopy (XPS) at various depths (XPS – depth profile).

We show that even at open circuit potential the fluorinated ether BTFEOE produces an ordered interphase leading to an SEI that better protects the a-Si anode than the non-fluorinated ether 1,2-DEE. We suggest that the -CF_3 end groups induce a steric effect or an electron repulsion[23] giving this fundamental finding. The SEI formed by the fluorinated electrolyte is thinner, more durable, and allows for increased Li diffusion[24] and subsequent deeper bulk alloying. Furthermore, a significantly different surface SEI composition with the addition of fluorinated electrolyte is revealed by SFG vibrational spectroscopy.

2. EXPERIMENTAL METHODS

2.1 Sum frequency generation vibrational spectroscopy.

The picosecond laser system consisted of a 1064 nm Nd:YAG pump laser (PL2250, Ekspla) with a repetition rate of 20 Hz and an average peak power of 25 mJ. A LaserVision optical parameter generator and amplifier system converted the 1064 nm to a visible 532 nm beam and a mid-IR beam ranging between 2200 cm^{-1} to 4000 cm^{-1}. SFG is achieved when a visible and an infrared beam overlap spatially and temporally on a medium[25] as shown in Scheme 1. The beam's orientation in all the SFG experiments was as follows: the angle of the 532 nm beam was 56˚ and the mid-IR beam was 45˚, in respect to the perpendicular plane to the sample surface (reference plane). We collected the SFG beam (in the UV range) by a Hamamatsu photomultiplier tube (Model R922); multiple irises are set along the SFG beam path and several band-pass filters are added to minimize the 532 nm light. Unless specified differently we used an *SSP* (SF,Vis,IR) polarization combination since it is sensitive to an adsorbate dipole moment perpendicular to the surface. The average power of 532 nm and mid-IR at 2950 cm^{-1} on the sample did not exceed 200 µJ, under the film's damage threshold.

2.2 Spectroelectrochemical half-cell

The spectroelectrochemical half-cell (ECC-OPTO-STD, EL-CELL), henceforth referred to as eCell, serves to monitor the optical properties of an electrode material in the course of electrochemical measurements. The working electrode material (WE) was amorphous Si anode. A 9 mm diameter lithium disc performs as both counter electrode (CE) and reference electrode (RE). All potentials are referred to the Li/Li^+ redox couple. The IR and visible beams shine from above through a CaF_2 window and the a-Si thin film. The SFG signal arising from the a-Si / electrolyte solution (solid/liquid) interface is reflected upwards in a back reflection mode. Prior to any experiment the eCell was dried over night at 80 C° in vacuum. We assembled (and disassembled) the eCell in an inert (ultra-pure argon) atmosphere with < 0.1-ppm concentration of water and oxygen (LabStar, MBruan). We performed cyclic-voltammetry (CV) as an electrochemical analytical technique using a VersaStat3 potentiostat (Princeton Applied).

Scheme 1. Our design of electrochemical half-cell (eCell) and anode facilitate in situ probing at the interface with SFG vibrational spectroscopy.

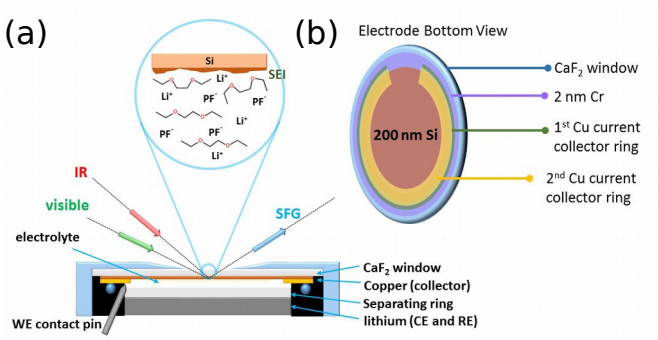

(a) General illustration of the electrochemical half-cell (eCell) for SFG measurement. (b) The layered amorphous Si anode and its copper current collectors deposited sequentially on a CaF_2 window. By depositing the copper rings and amorphous Si directly on the CaF_2 window we enable the visible and IR beams to propagate through the window and through the a-Si anode reaching the a-Si / electrolyte interface. The SFG signal then propagates upwards (back reflection). This design also ensures good electrical conductivity.

2.3 Anode preparation

We chose CaF_2 as the substrate in order to reduce IR absorption in the mid-IR (2200 cm^{-1} – 4000 cm^{-1}). By sequential mask deposition of 150 nm copper, 200 nm - 400 nm amorphous silicon thin film and 150 nm copper we have sandwiched the

a-Si working electrode (WE) between two copper rings. This enabled us to have reliable current collection[26] at the anodic potential of 0.005 V to 2.5 V vs Li/Li^+ (refer to Scheme 1). For general-purpose cyclic-voltammetry we used the same eCell only with 200 nm a-Si deposited on a 9 mm stainless steel disc.

2.4 X-ray photoelectron spectroscopy depth profile

Ex situ XPS measurements[27] were done in a PHI 5400 machine. It has a conventional (non-monochromatic) Al X-ray source (K_α=1486.7 eV) operated at 350 W. For depth profile analysis[28, 29], XPS survey spectra were acquired using analyzer pass energy of 178.5 eV, 1 eV step, 0.3 s dwell per step. The X-rays source was switched off during sputtering. For sputtering we used a gas fed differential ion gun (Physical Electronics). It produced Ar^+ ions beam at kinetic energy of 3 keV. The beam was at 40º in respect to the surface normal. We scanned the sample in a raster pattern over an area of ~ 3 mm x 3 mm. The beam current measured by an ammeter was approximately 14 mA. The sputtering rate was ~ 0.03 nm/sec. No sample rotation was used during sputtering.

2.3 Chemicals

The electrolyte was of battery-grade and consisted of 0.1 M Bis(trifluoromethane)sulfonimide lithium salt (LiTFSI) solvated in *either* 1,2-diethoxy ethane (1,2-DEE) *or* Bis(2,2,2-trifluoroethoxy) ethane (TOSOH F-TECH, INC), referred to as BTFEOE hence forth. The electrolyte solutions were used without further purification. Li foil was purchased from Sigma-Aldrich. Amorphous Si was deposited using an in house e-beam evaporator.

3. RESULTS AND DISSCUSSION

3.1 Sum frequency generation vibrational spectroscopy at open circuit potential

In Figure 1, we show the SFG spectra of 1,2-DEE and its fluorinated version (BTFEOE) with 0.1 M LiTFSI salt concentration in contact with the amorphous silicon anode when no external potential is applied, that is at open circuit potential (OCP). We have analyzed our experimental data according to an SFG intensity model in order to validate the peak assignments. The active SFG vibrations are summarized in Table 1. The SFG fitting model is described in detail in the Supporting Information section. To better identify methylene vibrations we named the methylene groups as follows (also refer to Scheme 2): α is bonded to an oxygen atom (-O-CH_2-), and β is bonded to an end group (-OCH_2-CX_3, X= H or F) and will be more affected by its electronegative nature.[30] Our FTIR vibrational peak assignments and analysis are described in Figure S3 and Table S1 in the Supporting Information section and are used to support SFG spectra analysis. However, vibrations that are IR active are not necessarily found in the SFG spectrum since a sum frequency vibration has to be active in both Raman and IR, also the phase of the sum frequency signal can induce a negative peak due to the interference with the SFG generated from the substrate.[13]

Scheme 2. The general chemical formula of the linear ethers (X = hydrogen or fluorine)

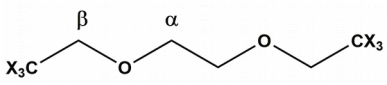

We have given the two methylene groups the following assignments according to their adjacent bonds: α as the -O-CH_2- backbone methylene and β as the -OCH_2-CX_3 end group.

In a glance the SFG profiles of both ethers are all but similar except for shoulders arising in the BTFEOE (*red curve*) profile at 2910 cm^{-1}, 2954 cm^{-1} and a dip at 2979 cm^{-1}.-

Table 1. Active SFG vibrations for 1,2-DEE and BTFEOE (fluorinated ether).

Assignments	1,2-DEE (cm^{-1})	BTFEOE (cm^{-1})
s-α-OCH_2	2850	2848
FR-α-OCH_2	2917	2923
as-α-OCH_2	2950	2955
s-β-OCH_2	2880	2877
FR-β-OCH_2	2941	2940
as-β-OCH_2	2981	2978
s-CH_3	2868	____

One of the advantages of SFG as a laser technique is gaining information on molecular orientation by employing specific polarization configurations. (See Supporting Information for details.). For example, electric field is either "*S*" polarized, perpendicular in respect to the substrate plane, or "*P*" polarized that is parallel to the substrate plane. There are 27 of surface susceptibility elements, $\chi^{(2)}_{s,ijk}$, but due to symmetrical redundancy these funnel into a few nonvanishing elements depending on the polarization combination.[13, 25, 31] In our study we are interested in the effect of fluorinated end groups on the electrolyte ether / a-Si interface, such as different adsorption angles at the liquid / solid interface. Therefore, we had applied an *SSP* (SFG, visible, IR) polarization combination which is more sensitive to the vibrations have net dipole

perpendicular to the substrate. The "rule of thumb" for a CH_2 stretching, the higher the intensity ratio between symmetric to asymmetric stretch the more upright position in respect to the substrate, in which the net dipole of CH_2 symmetric stretching point towards the direction perpendicular to the interface.[31, 32] In Figure 1, the 1,2-DEE (*black curve*) SFG intensities of the linear backbone, i.e., s-α-OCH_2 at 2850 cm^{-1} and as-α-OCH_2 at 2950 cm^{-1} modes are almost equal in intensity while only the s-β-OCH_2 at 2880 cm^{-1} is present. Linear ethers, like 1,2-DEE, have been shown to lie parallel to the interface while the terminal alkyl substituents are randomly turned towards the exterior of the solution phase or towards the substrate.[33] Free rotation and bending configuration results in zero SFG intensity, and hence, none of the symmetric and asymmetric -CH_3 vibrations are observed in the SFG spectra of 1,2-DEE. In the case of BTFEOE, (*red curve*) the linear backbone comprised out of two α methylene groups, -O-CH_2-CH_2-O-, still lies in parallel to the anode surface but due to the fluorinated methyl groups (–CF_3) mutual repulsion[23] and the fluorine affinity to the a-Si surface[34], the β-OCH_2 groups have lager tilted angle in respect to the surface plane and hence presumably BTFEOE molecule bend towards surface with fluorine end groups close to surface as we illustrate in Scheme 2. This is manifested by the higher intensity of the asymmetric α-OCH_2 at 2955 cm^{-1} compared with the s-α-OCH_2 at 2848 cm^{-1} and the lower amplitude s-β-OCH_2 at 2877 cm^{-1} vs the as-β-OCH_2 at 2978 cm^{-1}. Moreover, the narrower linewidth and higher intensity of the vibrations also gives evidence of a higher degree of ordering of surface molecules.

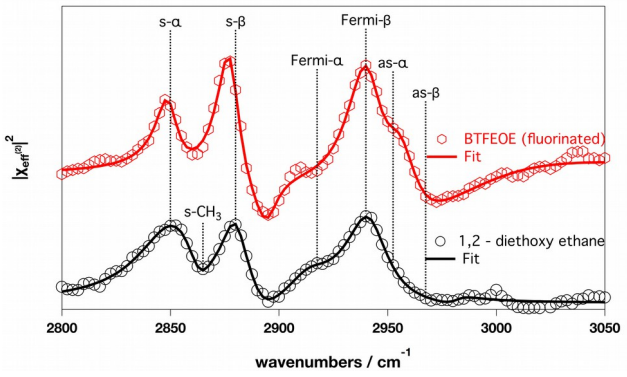

Figure 1. The SFG profiles of 0.1 M LiTFSI : 1,2-DEE (*black*) and 0.1 M LiTFSI : BTFEOE (*red*) in contact with amorphous Si anode at open circuit potential. We note the frequencies corresponding to α-OCH_2 (backbone) and β-OCH_2 (adjacent to –CX_3 end groups) methylene groups.

Scheme 3. An illustration of structures of the ethers adsorbed on a-Si at OCP

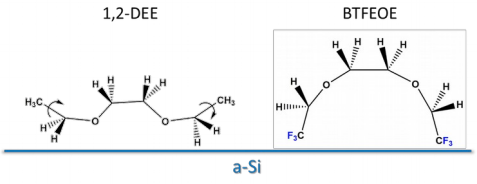

Left: the 1,2-DEE α-methylene groups (-O-CH_2-) lie close and in parallel to the a-Si anode surface while its -CH_3 groups are free to rotate and bend. *Right:* the BTFEOE, fluorinated ether, α-methylene groups (-O-CH_2-) have a more upright position and β-methylene (-OCH_2-CF_3) groups have higher tilted angle on the a-Si anode surface, a more ordered interface is observed.

3.2 SEM images and cyclic-voltammetry measurement

In Figure 2 we present ex situ SEM images of delithiated amorphous Si anodes after being cycled five times between 2.5 V to 0.005 V at a scan rate of 0.1 mV / sec. By probing the anode surfaces in their delithiated state after 5 full cycles, the SEI is thicker and so easier to probe.[35]

The SEM images show that the silicon anode surface is corrugated after cycling in 1,2-DEE (Figure 2a) whereas after cycling in BTFEOE (Figure 2b) the silicon anode surface is smooth. The smoother surface arises from the highly fluorinated reduction products having a lower surface energy[24, 36, 37] (and stereochemistry, refer to the SFG section). Chemically, the SEI formed from fluorinated ether reduction products having –CF_3 end groups might either induce a tighter and denser SEI layer[9] similar to the function of fluorinated additives[38] or an enriched anode surface with LiF[39] that lowers the surface diffusion energy[36, 40] of lithium atoms.[41] Another possibility is the formation of amorphous Si-F surface[42] which may lead to a more stable SEI since fluorine can shorten the length of oligomer chains present in the SEI layer, giving a more compact SEI film.[43] Hence, we suggest that lowering the surface energy[36] of the SEI will result in the increased lithium atoms surface diffusion on the Si anode leading to smoother surface features as can be seen in Figure 2b.

We have cycled the a-Si anode in both hydrocarbon and fluorinated electrolyte solutions at anodic potential ranges (0.005 V to 2.5 V) for 5 consecutive cycles. In Figure 3(a), 1,2-DEE, we can divide the CV potential range into two segments. The first potential range, between 2.5 V to 1.0 V has no reduction peaks and the current is relatively constant at ~ -10 □A. The second potential range, between ~ 0.9 V to 0.005 V, presents us with a two-step silicon lithiation (alloying with Li) process that has two peaks at 0.3 V (~ 28 □A) and 0.1 V (~ 80 □A). Below applied potentials of 0.5 V reduction pathways of linear ethers (e.g., dimethoxyethane, DME)[44] are possible and lithium alkoxides (e.g., $LiOCH_2CH_3$) are the dominant SEI product.[45]

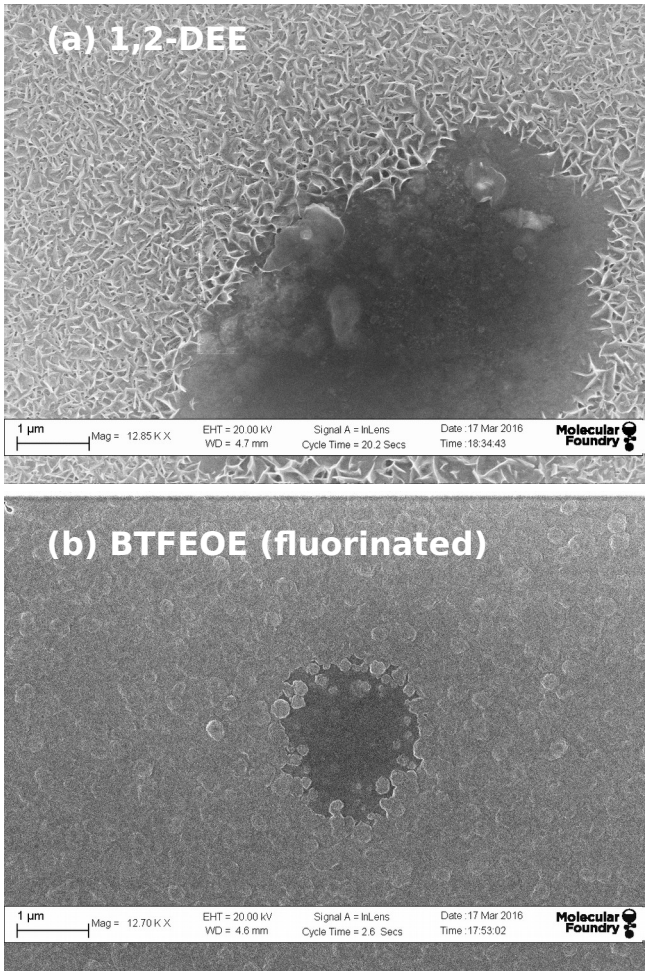

Figure 2. Fluorinated ether forms smoother SEI. SEM images of a-Si anodes after cycling them in (a) 1,2-DEE, the regular hydrocarbon ether and (b) BTFEOE, the fluorinated ether.

We suggest that the two peaks (at 0.3 V and 0.1 V) are a two-step lithiation process since the amount of charge calculated from the anodic peak at 0.3 V could only match a lithium silicon alloying process. Notably, the lithiation peak at 0.3 V is not present in the first cycle (Figure 2a, *black curve*), bellow 1.0 V the current increases gradually until reaching a peak of roughly – 80 μA at 0.05 V (lithiation).[46] When discharging the a-Si anode, by ramping the applied potential from 0.005 V to 2.5 V we detect two cathodic peaks at 0.36 V and 0.57 V. We associate them with the bulk delithiation of the silicon anode.[46, 47] Between the second CV and fifth CV the current values of the scans at the delithiation potentials (0.36 V and 0.57 V) are erratic ranging from 11 μA to 30 μA at 0.36 V and 34 μA to 80 μA around 0.57 V. Thus, we assume that the SEI could not mitigate silicon desolation due to bulk volume contraction as the lithium was extracted from the silicon bulk. Consequently, fresh silicon surface was exposed and further electrolyte was decomposed on the anodes surface.

In Figure 3b, BTFEOE fluorinated ether, we show 5 consecutive CV profiles of 0.1 M LiTFSI dissolved in BTFEOE between 2.5 V to 0.005 V. Between 2.5 V to 1.0 V no significant reduction occurs and the current is relatively constant at ~ -11 μA. Between ~ 0.9 V to 0.005 V, we see the lithium silicon alloying process. In the first scan (black curve) the CV profile shows a single lithiation stage at ~ 0.1 V (~ 80 μA) and delithiation at ~ 0.5 V. Thereafter, CV scan profiles (2 – 5) have two peaks at 0.3 V (~ 29 μA) and 0.1 V (~ 60 μA) that we assign to a two-step lithiation process as the amount of charge calculated from the anodic peak at 0.3 V could only match a lithium silicon alloying process.[46] Upon reversing the potential from 0.005 V to 2.5 V, we assign 0.3 V and 0.55 V as the cathodic peaks associated with delithiation.[47] We deduce that in fluorinated ether solution (BTFEOE) the SEI is able to reduce the physical deterioration of the Si anode since the 2nd to 5th CV profiles converge.

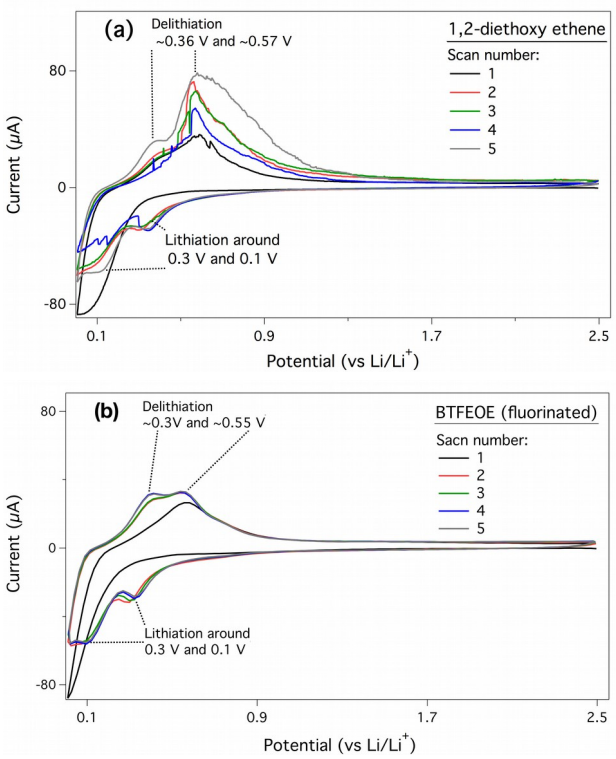

Figure 3. We present 5 lithiation / delithiation cycles of 200 nm amorphous Si anode as CVs of (a) 0.1 M LiTFSI : 1,2-DEE and (b) 0.1 M LiTFSI : BTFEOE, the fluorinated version of 1,2-DEE. The scan rate for all CVs was 0.1 mV / sec.

3.3 Sum frequency generation vibrational spectroscopy under working conditions

In Figure 4a and 4b we present the divided SFG spectra of 1,2-DEE and BTFEOE after applying a dynamic potential (i.e., cyclic-voltammetry, CV) by dividing the SFG spectra (SFG_{CV} / SFG_{OCP}) to emphasize the appearance (or trend) of vibrational peaks that are less clear in a regular SFG scan. In Figure S8 and S9 we present the nondivided SFG spectra of 1,2-DEE and BTFEOE after CV. We have also carried out fitting in order to identify the redox surface species from the a-

Si/SEI interface. We have divided the cycling range into two potential segments. In the first, we cycled the amorphous silicon anode between 0.8 V to 1.1 V, hereafter referred to as "CV ~ 1 V", where no major reduction pathways were detected in the CV. In the second range, we cycled the a-Si anode between 0.9 V to 0.005 V, hereafter referred to as "lithiation". In this potential range both reduction of the electrolyte and lithiation of the bulk silicon occurs. Scan rates for all cycling were 0.1 mV / sec.

The SFG trend profiles of 1,2-DEE (Figure 4a) and BTFEOE (Figure 4b) after cycling are different. Hence, we assume that two different end products were formed via two different reduction mechanisms. When examining Figure 4a, the SFG trend after CV ~1 V in 1,2-DEE (*full blue dot*), we can see that peaks of the symmetric α-OCH_2 (~2850 cm^{-1}) have intensified after lithiation (*green curve*). We suggest that the ether has decomposed and its moieties formed silicon carbon bonds.[18],[48],[49] Amorphous Si has surface features of both Si-O_x and Si-H termination, as determined by SFG (Figure 1S) and XPS.[50] We suggest that the shoulder at ~ 2940 cm^{-1} originates from a homolytic beta cleavage of the ether[51] resulting in a radical that quickly reacts with the a-Si (having features of Si-H termination) to produce a mixture of Si-OCH_2-CH_3 or Si-O-CH_2-CH_2-OCH_2-CH_3 terminations. We assign the peak at ~2880 cm^{-1} to the symmetric stretch of a s-β-OCH_2 (methylene group adjacent to the methyl group, -OCH_2-CH_3). With respect to our spectral resolution (3 cm^{-1}) the α-OCH_2 and β-OCH_2 frequencies do not significantly change after lithiation but do intensify (refer to Table S1 in the Supporting Information). The similar peak frequencies of the SFG profile being intensified upon lithiation, and the fact that no new peaks arise after lithiation, tell us that the same SEI compound is formed at CV ~ 1V and lithiation.

In Figure 4b we show the SFG trend spectra of the fluorinated ether (BTFEOE) after CV ~ 1 V (*full blue dot*) and lithiation (*green curve*). For BTFEOE the SFG spectrum shows permanent change after lithiation and a different SEI composition from the one obtained after CV ~ 1 V. After performing a CV ~ 1 V some reduction takes place but the main reduction occurs only below ~ 0.5 V. This is apparent in the SFG spectrum; for example, the symmetrical stretch, α-OCH_2 peak (2850 cm^{-1}) is more noticeable after lithiation. Its amplitude intensifies after lithiation, which is presumed to be due to the increased decomposition of electrolyte on the lithiated surface. There are also a few moderate peaks at 2907 cm^{-1} and 2942 cm^{-1} that we assign to Fermi α-OCH_2 and Fermi β-OCH_2, respectively. After lithiation there are major changes that correspond to symmetric s-Si-β-OCH_2 (2877 cm^{-1}) that we propose arise from Si-OCH_2-CH_3 or Si-O-CH_2-CH_2-OCH_2-CH_3 terminations. We detect Fermi β contributions at 2938 cm^{-1} and an asymmetric β-OCH_2 after at 2963 cm^{-1}. Finally, only after lithiation we detect two broad peaks at 2983 cm^{-1} and 3024 cm^{-1} that we attribute to the appearance of an unconjugated fluoroalkene group (R–O–**CH**=CF_2), a reported product of the beta cleavage that intensifies after lithiation.[18, 51, 52] Therefore, we suggest that the a-Si surface may now be covered with Si-O-CH_2-CH_2-O-CH=CF_2 and Si-OCH_2-CF_3.

Our main conclusion from the SFG spectra is that for 1,2-DEE the SEI formed at ~ 1V is the same as the one formed after lithiation and this product is apparent in the SFG spectra. For BTFEOE a new SEI component (presumably fluorinated olefin or alkane) appears only *after* lithiation.-

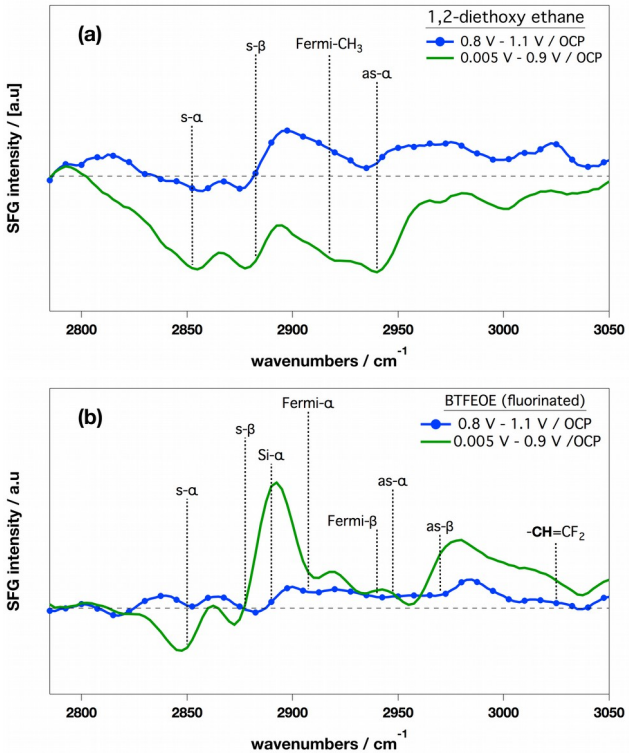

Figure 4. SFG trend analysis (SFG_{CV} / SFG_{OCP}) spectra obtained after cycling at 1.1 V – 0.8 V (CV ~ 1 V, *full blue dot*) and after 0.05 V – 0.9 V (lithiation, *green*) for (a) 1,2-DEE and (b) BTFEOE, the fluorinated ether.

3.4 Depth profile XPS

We have also performed ex situ X-ray photoelectron spectroscopy (XPS) measurements and depth profile XPS in order to understand the extent of a-Si lithiation.[53] In Figure 5a we present XPS depth profiling of a-Si in its lithiated state after it was cycled 5 times between 2.5 V to 0.05 V at 0.1 mV / second in 0.1 M LiTFSI : 1,2-DEE based electrolyte. At zero depth we assign the amorphous silicon electrolyte solution interface. The sputter rate was constant and equaled 0.03 nm / sec. Therefore, after sputtering for approximately 200 minutes we have roughly removed 200 nm of bulk silicon. This was verified both by XPS detection of iron $2p_{3/2}$ signal,

implying that we have reached the stainless-steel substrate, and by AFM measurements (Figure S2). The first three depth XPS scans were performed at 3-minute intervals, corresponding to a ~5.5 nm sputtered layer removed. Later XPS depth sputtering scans were taken with ~10 minute intervals (~ 18 nm). In Figure 5a, the depth profile of the 1,2-DEE system, the lithium atomic percentage (black full dot) on the a-Si surface is ~30 % and increases to 65 % at ~20 nm away from the a-Si surface. From 20 nm to 58 nm the Li atomic percentage decreases to zero. We chose to probe the signals of O 1s (open blue square) and Si 2p (full green square) in order to follow the a-Si thin film. It seems that when Li atomic concentration is above 30 % the atomic surface concentration of oxygen and silicon remain below 15 %. Once the atomic concentration of Li falls below 30 % the O 1s and Si 2p signals rise to 30 % and 60 %, respectively. This supports the general idea that during lithiation and delithiation the Si anode undergoes tremendous volume expansions and contractions, consequently leading to the anode's desolation. More to the point, it reveals something on the Li alloying (lithiation) depth. Combined with the CV data from Figure 2a we can deduce that the SEI cannot maintain the integrity of the Si anode thin film. Fluorine (open red dot) presence is around 15 % about 5 nm deep and from there on its surface concentration dwindles to zero at 68 nm deep. We assume it originates from adsorbed anion salt (TFSI).

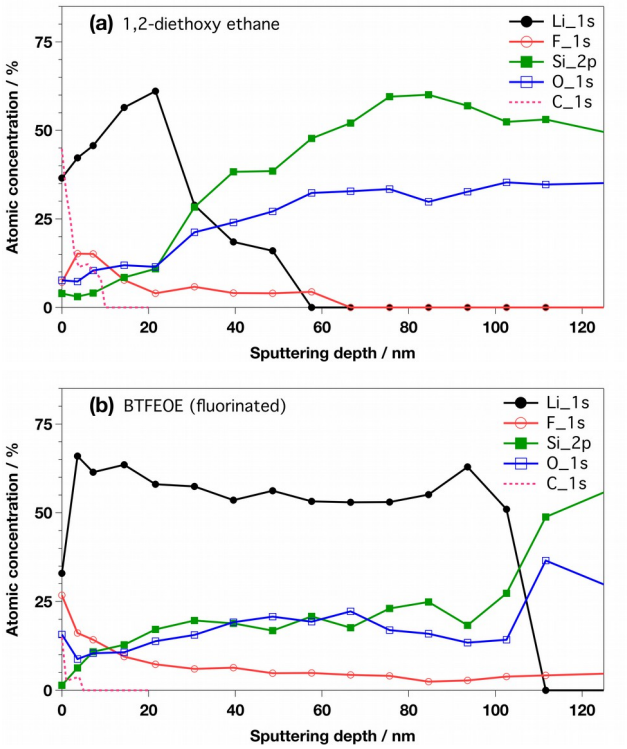

Figure 5. We present elemental XPS depth profiles (atomic concentration vs. nm) of lithium (*full black dot*), fluorine (*open red dot*), silicon (*full green square*), oxygen (*open blue square*) and carbon (*dashed pink line*) in amorphous Si anodes after 5 CVs in (a) 1,2-DEE or (b) BTFEOE (the fluorinated ether). The sputter rate was 0.03 nm / sec. At zero depth we assign the amorphous silicon electrolyte solution interface.

Lastly, we probed the carbon C 1s (dashed pink line) signal as a qualitative estimate to the solid electrolyte interphase thickness formed by the 1,2-DEE based electrolyte after the first 5 lithiation / delithiation cycles. The relative carbon concentration on the a-Si surface is ~ 45 %, after which it drops to 12% at a sputtering depth of ~ 4 nm. At a sputtering depth of 10 nm, the carbon signal has completely disappeared; we therefore assume that for 1,2-DEE the thickness of the SEI is 10 nm.

In Figure 5b, we present the XPS depth profile of lithiated a-Si after cycling it 5 times in BTFEOE (fluorinated ether) electrolyte. The depth profiling procedure is the same as for the 1,2-DEE. Interestingly, in the fluorinated ether the Li (full black dot) seems to intercalate up to 100 nm which is half the thickness of the a-Si anode (200 nm). The atomic percentage of lithium on the surface is ~ 30 %. Nevertheless, within 5 nm it shoots to 68 % and later in the bulk anode it is 60 % in average. As we further sputter away a-Si layers we discover by XPS that the Li concentration reaches 50% of the elemental abundance. As with 1,2-DEE as long as the atomic surface concentration of Li is above 30 % both silicon (full green square) and oxygen (open blue square) surface concentrations are below 25 %. At 110 nm the Li percentage plummets to zero and the O 1s and Si 2p reach 36 % and 48 % atomic concentrations, respectively. The fluorine (open red dot) atomic percentage on the surface is 25 %, within 20 nm is reduced to ~ 10 %, and monotonically decreases to ~ 5 % throughout the sputtering process. It seems that Li intercalates deeper when the fluorine-based SEI is formed. Lastly, the C 1s (dashed pink line) signal was probed as a qualitative estimate to the solid electrolyte interphase thickness formed by the BTFEOE (fluorinated ether) based electrolyte after the first 5 lithiation / delithiation cycles. The relative carbon concentration on the a-Si surface is ~ 15 %; it sharply decreases to ~ 3 % after an equivalent sputter of ~ 3 nm. Finally, the signal decays to zero after sputtering 5 nm. We therefore assume that for fluorinated ether, BTFEOE, the thickness of the SEI is 5 nm. As reported in the past, fluorinated SEI should be thinner than an SEI formed from the regular hydrocarbons.[38] This trend is evident in our ether based electrolytes as the SEI formed by 1,2-DEE (~10nm thickness) is almost double the SEI formed by BTFEOE of ~5nm.

Combining our SFG and XPS data we deduce that the reason BTFEOE (fluorinated ether) forms a stable SEI below 0.9 V is that as a linear ether it has a somewhat perpendicular orientation in respect to the a-Si plane that is induced by its

fluorinated methyl groups (section 1 - SFG). We suggest that this orientation lowers the lithium ion diffusion energy through the SEI and thus enables deeper bulk alloying as detected by XPS depth analysis (section 5 - XPS).

5. CONCLUSIONS

In conclusion, we suggest that the fundamental reason for the beneficial effect of fluorinated electrolytes is due to their ability to form an ordered interphase at open circuit potential. In summary, the electrolyte BTFEOE – the fluorinated version of 1,2-DEE – forms an interface that has features which are perpendicular to the amorphous Si anode surface at open circuit potential resulting in a stable SEI. This stable SEI created by the fluorinated electrolyte allows for deeper Li diffusion and alloying while better maintaining the integrity of the Si anode film. In the future we will look at the effect of fluorination in carbonate based electrolyte solutions and the resulting solid electrolyte interphase.

ASSOCIATED CONTENT

Supporting Information

The Supporting Information is available free of charge on the ACS Publications website.

SFG of amorphous silicon, AFM profile, FTIR spectra and analysis

AUTHOR INFORMATION

Corresponding Author

[$] Somorjai@berkeley.edu

Author Contributions

The authors declare no competing financial interest.
[*] Y.H and H-L. H contributed equally to this work.

Notes

Any additional relevant notes should be placed here.

ACKNOWLEDGMENT

This work was supported by the Assistant Secretary for Energy Efficiency and Renewable Energy, Office of Freedom CAR and Vehicle Technologies of the U.S. Department of Energy under Contract No. DE-AC02 O5CH1123. The SFG instrumentation was purchased with funding from the Director, Office of Basic Energy Sciences, Materials Science and Engineering Division of the U.S. Department of Energy. XPS and TEM measurements were conducted at the Molecular Foundry (Proposal #3806). Y. H. was graciously funded through a grant from Honda Research Institute. We would also like to thank A. Buyanin for his AFM work.

REFERENCES

[1] E. Peled, Journal of the Electrochemical Society 1979, 126, 2047.

[2] F. Shi, P. N. Ross, H. Zhao, G. Liu, G. A. Somorjai, K. Komvopoulos, J Am Chem Soc 2015, 137, 3181.

[3] P. N. Ross, Catal Lett 2014, 144, 1370.

[4] M. A. McArthur, S. Trussler, J. R. Dahn, Journal of the Electrochemical Society 2012, 159, A198.

[5] S. Dalavi, P. Guduru, B. L. Lucht, Journal of The Electrochemical Society 2012, 159, A642.

[6] K. Xu, Chem Rev 2004, 104.

[7] K. Xu, Chem Rev 2014, 114, 11503.

[8] J. M. Garcia, H. W. Horn, J. E. Rice, J Phys Chem Lett 2015, 6, 1795; B. Genorio, J. Staszak-Jirkovský, R. S. Assary, J. G. Connell, D. Strmcnik, C. E. Diesendruck, P. P. Lopes, V. R. Stamenkovic, J. S. Moore, L. A. Curtiss, N. M. Markovic, The Journal of Physical Chemistry C 2016.

[9] X.-B. Cheng, R. Zhang, C.-Z. Zhao, F. Wei, J.-G. Zhang, Q. Zhang, Advanced Science 2016, 3, 1500213.

[10] D. Aurbach, Z. Lu, A. Schechter, Y. Gofer, H. Gizbar, R. Turgeman, Y. Cohen, M. Moshkovich, E. Levi, Nature 2000, 407, 724; C. B. Bucur, T. Gregory, A. G. Oliver, J. Muldoon, The Journal of Physical Chemistry Letters 2015, 6, 3578.

[11] D. Guyomard, J. M. Tarascon, Journal of Power Sources 1995, 54, 92.

[12] D. E. Arreaga-Salas, A. K. Sra, K. Roodenko, Y. J. Chabal, C. L. Hinkle, The Journal of Physical Chemistry C 2012, 116, 9072.

[13] Y. R. Shen, Nature 1989, 337, 519.

[14] H. J. Liu, Y. J. Tong, N. Kuwata, M. Osawa, J. Kawamura, S. Ye, J Phys Chem C 2009, 113, 20531.

[15] L. Yu, H. Liu, Y. Wang, N. Kuwata, M. Osawa, J. Kawamura, S. Ye, Angew Chem Int Ed Engl 2013, 52, 5753.

[16] P. Mukherjee, A. Lagutchev, D. D. Dlott, Journal of the Electrochemical Society 2012, 159, A244.

[17] B. G. Nicolau, N. García-Rey, B. Dryzhakov, D. D. Dlott, The Journal of Physical Chemistry C 2015, 119, 10227.

[18] Y. Horowitz, H. L. Han, P. N. Ross, G. A. Somorjai, Journal of the American Chemical Society 2016, 138, 726.

[19] D. Alves Dalla Corte, G. Caillon, C. Jordy, J.-N. Chazalviel, M. Rosso, F. Ozanam, Advanced Energy Materials 2016, 6, n/a.
[20] X. Wang, F. Fan, J. Wang, H. Wang, S. Tao, A. Yang, Y. Liu, H. Beng Chew, S. X. Mao, T. Zhu, S. Xia, Nat Commun 2015, 6, 8417.
[21] L. Y. Beaulieu, K. W. Eberman, R. L. Turner, L. J. Krause, J. R. Dahn, Electrochem Solid St 2001, 4, A137.
[22] T. D. Hatchard, J. R. Dahn, Journal of The Electrochemical Society 2004, 151, A838.
[23] Y. Sasaki, G. Shimazaki, N. Nanbu, M. Takehara, M. Ue, ECS Transactions 2009, 16, 23.
[24] M. Jäckle, A. Groß, The Journal of Chemical Physics 2014, 141, 174710.
[25] C. D. Bain, Journal of the Chemical Society, Faraday Transactions 1995, 91, 1281.
[26] S.-T. Myung, Y. Hitoshi, Y.-K. Sun, Journal of Materials Chemistry 2011, 21, 9891.
[27] P. v. d. Heide, *X-Ray Photoelectron Spectroscopy: An Introduction to Principles and Practices*, Jon Wiley & Sons, 2012.
[28] C. J. Powell, A. Jablonski, Journal of Electron Spectroscopy and Related Phenomena 2010, 11.
[29] R. Behrisch, W. Eckstein, *Sputtering by particle bombardment : experiments and computer calculations from threshold to MeV energies*, Springer, Berlin ; New York 2007.
[30] B. H. Stuart, *Infrared Spectroscopy: Fundamentals and Applications*, Wiley, 2004; G. Socrates, *Infrared and Raman Characteristic Group Frequencies: Tables and Charts*, John Wiley & Sons, 2004.
[31] H. Xu, D. Zhang, J. Hu, C. Tian, Y. R. Shen, The Journal of Physical Chemistry A 2015, 119, 4573.
[32] Y. D. Su, H. L. Han, Q. Cai, Q. Wu, M. X. Xie, D. Y. Chen, B. S. Geng, Y. B. Zhang, F. Wang, Y. R. Shen, C. S. Tian, Nano Letters 2015, 15, 6501.
[33] A. Daghetti, S. Trasatti, I. Zagorska, Z. Koczorowski, Electrochimica Acta 1988, 33, 1705.
[34] C. J. Wu, E. A. Carter, Physical Review B 1992, 45, 9065.
[35] G. M. Veith, M. Doucet, J. K. Baldwin, R. L. Sacci, T. M. Fears, Y. Q. Wang, J. F. Browning, J Phys Chem C 2015, 119, 20339.
[36] P. W. Hoffmann, M. Stelzle, J. F. Rabolt, Langmuir 1997, 13, 1877.
[37] Q. Chen, K. Geng, K. Sieradzki, Journal of The Electrochemical Society 2015, 162, A2004.
[38] I. A. Shkrob, J. F. Wishart, D. P. Abraham, The Journal of Physical Chemistry C 2015, 119, 14954.
[39] Y. Zhang, J. Qian, W. Xu, S. M. Russell, X. Chen, E. Nasybulin, P. Bhattacharya, M. H. Engelhard, D. Mei, R. Cao, F. Ding, A. V. Cresce, K. Xu, J. G. Zhang, Nano Lett 2014, 14, 6889.
[40] M. Jackle, A. Gross, J Chem Phys 2014, 141, 174710.
[41] C. Monroe, J. Newman, Journal of The Electrochemical Society 2003, 150, A1377; Y. Lu, Z. Tu, L. A. Archer, Nat Mater 2014, 13, 961.
[42] H. Zhou, J. Nanda, S. K. Martha, R. R. Unocic, H. M. Meyer, 3rd, Y. Sahoo, P. Miskiewicz, T. F. Albrecht, ACS Appl Mater Interfaces 2014, 6, 7607.
[43] D. P. Abraham, M. M. Furczon, S. H. Kang, D. W. Dees, A. N. Jansen, Journal of Power Sources 2008, 180, 612.
[44] D. Aurbach, M. L. Daroux, P. W. Faguy, E. Yeager, Journal of the Electrochemical Society 1988, 135, 1863.
[45] A. L. Michan, G. Divitini, A. J. Pell, M. Leskes, C. Ducati, C. P. Grey, Journal of the American Chemical Society 2016.
[46] J. Yang , N. Solomatin, A. Kraytsberg, Y. Ein-Eli ChemistrySelect 2016, 1, 572.
[47] K. W. Schroder, H. Celio, L. J. Webb, K. J. Stevenson, J Phys Chem C 2012, 116, 19737.
[48] D. J. Michalak, S. R. Amy, A. Esteve, Y. J. Chabal, J Phys Chem C 2008, 112, 11907.
[49] D. J. Michalak, S. R. Amy, D. Aureau, M. Dai, A. Esteve, Y. J. Chabal, Nat Mater 2010, 9, 266.
[50] K. W. Schroder, A. G. Dylla, S. J. Harris, L. J. Webb, K. J. Stevenson, ACS Applied Materials & Interfaces 2014, 6, 21510.
[51] S. L. BERNAS, R. GRAHAMCOOK, Organic Mass Spectrometry 1970, 3, 3.
[52] V. K. Thakur, E. J. Tan, M.-F. Lin, P. S. Lee, Journal of Materials Chemistry 2011, 21, 3751.
[53] J. Maibach, F. Lindgren, H. Eriksson, K. Edstrom, M. Hahlin, J Phys Chem Lett 2016, 7, 1775.

Insert Table of Contents artwork here